



Intelligent nanogels with self-adaptive responsiveness for improved tumor drug delivery and augmented chemotherapy

Xin Li^{a,b,d,1}, Helin Li^{b,d,1}, Changchang Zhang^c, Andrij Pich^{b,d,f,*}, Lingxi Xing^{a,**}, Xiangyang Shi^{c,e,***}

^a Department of Gynecology and Obstetrics, XinHua Hospital Affiliated to Shanghai JiaoTong University School of Medicine, Shanghai, 200092, China

^b DWI-Leibniz-Institute for Interactive Materials e.V., 52056, Aachen, Germany

^c College of Chemistry, Chemical Engineering and Biotechnology, Donghua University, Shanghai, 201620, China

^d Institute for Technical and Macromolecular Chemistry, RWTH Aachen University, 52074, Aachen, Germany

^e CQM-Centro de Química da Madeira, Universidade da Madeira, Campus da Penteada, 9000-390, Funchal, Portugal

^f Aachen Maastricht Institute for Biobased Materials, Maastricht University, 6167, RD Geleen, Netherlands

ARTICLE INFO

Keywords:

Ultrafast charge conversion

Nanogels

Active transportation

Deep tumor penetration

Enhanced antitumor activity

ABSTRACT

For cancer nanomedicine, the main goal is to deliver therapeutic agents effectively to solid tumors. Here, we report the unique design of self-adaptive ultrafast charge-reversible chitosan-polypyrrole nanogels (CH-PPy NGs) for enhanced tumor delivery and augmented chemotherapy. CH was first grafted with PPy to form CH-PPy polymers that were used to form CH-PPy NGs through glutaraldehyde cross-linking via a miniemulsion method. The CH-PPy NGs could be finely treated with an alkaline solution to generate ultrafast charge-reversible CH-PPy-OH-4 NGs (R-NGs) with a negative charge at a physiological pH and a positive charge at a slightly acidic pH. The R-NGs display good cytocompatibility, excellent protein resistance, and high doxorubicin (DOX) loading efficiency. Encouragingly, the prepared R-NGs/DOX have prolonged blood circulation time, enhanced tumor accumulation, penetration and tumor cell uptake due to their self-adaptive charge switching to be positively charged, and responsive drug delivery for augmented chemotherapy of ovarian carcinoma *in vivo*. Notably, the tumor accumulation of R-NGs/DOX (around 4.7%) is much higher than the average tumor accumulation of other nanocarriers (less than 1%) reported elsewhere. The developed self-adaptive PPy-grafted CH NGs represent one of the advanced designs of nanomedicine that could be used for augmented antitumor therapy with low side effects.

1. Introduction

Nanomedicine has been continuously developed to efficiently deliver diagnostic and therapeutic agents to solid tumors [1–3]. However, only approximately 1% of agents can be delivered to the targeted tumor cells after intravenous injection since they encounter considerable biological barriers during the delivery process [4–6]. This is the reason why numerous nanocarriers are effective in experimental models, but the results of clinical trials are unsatisfactory [7,8]. Therefore, it is urgently

needed to develop novel nanocarriers for efficient drug delivery with enhanced therapeutic efficacy *in vivo*.

To overcome the biological barriers, a variety of nanocarriers have been designed properly with different properties (e.g., particle size, surface charge and functional modification) [9–11]. Despite this, most of the nanocarriers are still suboptimal in biomedical applications. Normally, the nanocarriers with a small size [12], positive charge [13] and/or targeting molecules [14] are capable of improving tumor penetration and cellular internalization, respectively because of the strong or

Peer review under responsibility of KeAi Communications Co., Ltd.

* Corresponding author. DWI-Leibniz-Institute for Interactive Materials e.V., 52056, Aachen, Germany.

** Corresponding author. Department of Gynecology and Obstetrics, XinHua Hospital Affiliated to Shanghai JiaoTong University School of Medicine, Shanghai, 200092, China

*** Corresponding author. College of Chemistry, Chemical Engineering and Biotechnology, Donghua University, Shanghai, 201620, China.

E-mail addresses: pich@dwil.rwth-aachen.de (A. Pich), xinglingxi@xinhumed.com.cn (L. Xing), xshi@dhu.edu.cn (X. Shi).

¹ X. Li and H. Li contributed equally to this work.

<https://doi.org/10.1016/j.bioactmat.2021.03.021>

Received 12 December 2020; Received in revised form 23 February 2021; Accepted 10 March 2021

2452-199X/© 2021 The Authors. Publishing services by Elsevier B.V. on behalf of KeAi Communications Co. Ltd. This is an open access article under the CC

BY-NC-ND license (<http://creativecommons.org/licenses/by-nc-nd/4.0/>).

specific interactions with cell membranes, but they are often subjected to accelerated clearance by the kidney [15] or reticuloendothelial system (RES) [16], resulting in short half-life and insufficient tumor accumulation [17]. Likewise, the nanocarriers with a large size [18], neutral/negative charge [19] and/or hydrophilic coating (such as, polyethylene glycol (PEG) or zwitterions) [20,21] may accumulate effectively into the tumors attributing to the passive enhanced permeability and retention (EPR) effect, excellent stability and prolonged circulation time in the blood, respectively, while the cellular internalization of these nanocarriers is unacceptable due to the limited cell interactions [22–24].

In recent years, two major innovative strategies have been developed to improve the delivery efficacy of nanocarriers. Firstly, the modulation of tumor extracellular matrix (ECM) using the degrading enzymes (e.g., hyaluronidase) has been introduced to reduce the interstitial fluid pressure and the hindrance of obstacles [25]. While, the uncontrollable disintegration of ECM may lead to various unexpected risks (e.g., musculoskeletal pain, promoted tumor progression or even metastasis) [26,27]. Secondly, stimuli-responsive nanocarriers that exhibited size-switchable (large to small) or charge-reversible behavior (neutral/negative to positive) under different microenvironments *in vivo* were properly designed to prolong the blood circulation, enhance tumor accumulation or elevate cellular internalization for improved tumor treatment [28–30].

Remarkably, in a very recent work, Chan et al. [31] proved that 97% of nanoparticles were transported into solid tumors using active process through transcytosis rather than EPR effect or passive diffusion through tissue gaps. Moreover, Shen et al. [32,33] designed enzyme-triggered charge-reversal polymers by thioketal linker cleavage to improve tumor deep penetration, cellular internalization and anticancer activity using active transportation. These latest and important discoveries demonstrate that the efficient delivery of nanocarriers mainly depends on the surface charge (active transportation) instead of particle size (EPR effect or passive diffusion), and the charge-reversal nanocarriers are the most promising candidates to overcome biological barriers through the active transportation for efficient drug delivery and tumor treatment [34]. Meanwhile, the new opportunities and challenges of cancer nanomedicine require the development of novel self-adaptive ultrafast charge-reversal nanocarriers to address the issue of timeline of changeable process.

Normally, the charge-reversible nanocarriers are created by stimuli-triggered protonation/deprotonation or covalent bond cleavage of the major functional groups of the carriers. Some pH-responsive charge-reversible assemblies have been prepared through the hydrophobic self-assembly [35]. Although the surface charge conversion can be achieved through protonation under an acidic condition, the assembled structure is also destroyed due to the increase of their hydrophilicity. Moreover, this strategy is not suitable to prepare nanogels (NGs) owing to the hydrophobicity of the polymers. Currently, the preparation of NGs having a charge conversion from neutral to positive through protonation only has limited success [36]. Instead, it is relatively easy to prepare NGs having a surface charge conversion from negative to positive [37–40]. In any case, the process of stimuli-triggered cleavage of chemical bonds usually takes hours to complete and the NGs may have been cleared before the desired stimuli-triggering process, leading to limited drug delivery and treatment efficacy [41]. Therefore, it is extremely urgent to develop novel smart NGs with charge conversion from negative to positive through a facile method.

Here, we designed the self-adaptive ultrafast charge-reversible chitosan-poly pyrrole nanogels (CH-PPy NGs) by a facile method to simultaneously prolong the blood circulation time, improve tumor penetration and promote cellular internalization for augmented chemotherapy of ovarian carcinoma. The CH-PPy polymers were first synthesized using CH and pyrrole (Py) as building blocks, and cross-linked using glutaraldehyde (GA) *via* a miniemulsion method to form the CH-PPy NGs (P-NGs) with enzymatic degradability. Next, through facile

treatment by an alkaline solution, the pH-triggered charge-reversal CH-PPy-OH-4 NGs (R-NGs) were obtained. The NGs were used to load anticancer drug doxorubicin (DOX). We systematically characterized the NGs synthesis, surface charge change, optical property in near-infrared (NIR) region, protein resistance, biodegradation and stimuli-responsive drug release. The biocompatibility, tumor spheroid penetration, cellular internalization, pharmacokinetics, tumor accumulation and antitumor activity *in vivo* were next evaluated. The major hypothesis of the study is as follows: The initial R-NGs with surface negative charge display prolonged blood circulation time, and once the R-NGs accumulate in the tumor tissue, their surface charge converts to be positive through rapid protonation of Py ring to facilitate deep tumor penetration and cellular internalization *via* active transportation for improved chemotherapy of tumors (Scheme 1). To our knowledge, this is the very first report related to the design of self-adaptive charge-switchable CH-PPy-based NGs for augmented anticancer chemotherapy applications.

2. Experimental section

2.1. Preparation of CH-PPy polymers, CH-PPy NGs and CH-PPy-OH NGs

Py (20.8 mg/mL, 5 mL in 1 M HCl) and APS (70.8 mg/mL, 2.5 mL in 1 M HCl) were added dropwise to a CH solution (10 mg/mL, 5 mL in 0.1 M acetic acid), respectively under stirring at 0 °C in the dark for 1 h, and then the solution was stirred at room temperature for another 24 h. The reaction was stopped and the polymers were precipitated by addition of ethanol (200 mL), and further purified by centrifugation and washing by ethanol for 3 times to remove unreacted Py. Finally, the product was dried in the oven at 60 °C for 2 days to obtain the CH-PPy polymers. To generate CH-PPy polymers with a lower modification degree of PPy (CH-PPy-L), the initial amounts of Py and APS were lowered to be 4.2 mg/mL (in 5 mL in 1 M HCl) and 14.1 mg/mL (in 2.5 mL in 1 M HCl) while keeping other parameters and reaction conditions fixed.

CH-PPy or CH-PPy-L NGs were prepared by an inverse miniemulsion method using CH-PPy or CH-PPy-L polymers (10 mg/mL, 1 mL in 1 M HCl) and GA (10 μ L) as an aqueous phase, and Span-80 (25.8 mg/mL, in 10 mL cyclohexane) as an organic phase. The mixture was ultrasonicated by a Misonix Sonicator (XL2000, Division of QSonica, LLC., Newtown, CT) at the duty cycle of 50% and output control of 40% under the ice-cooling for 10 min, and then was stirred at room temperature overnight.

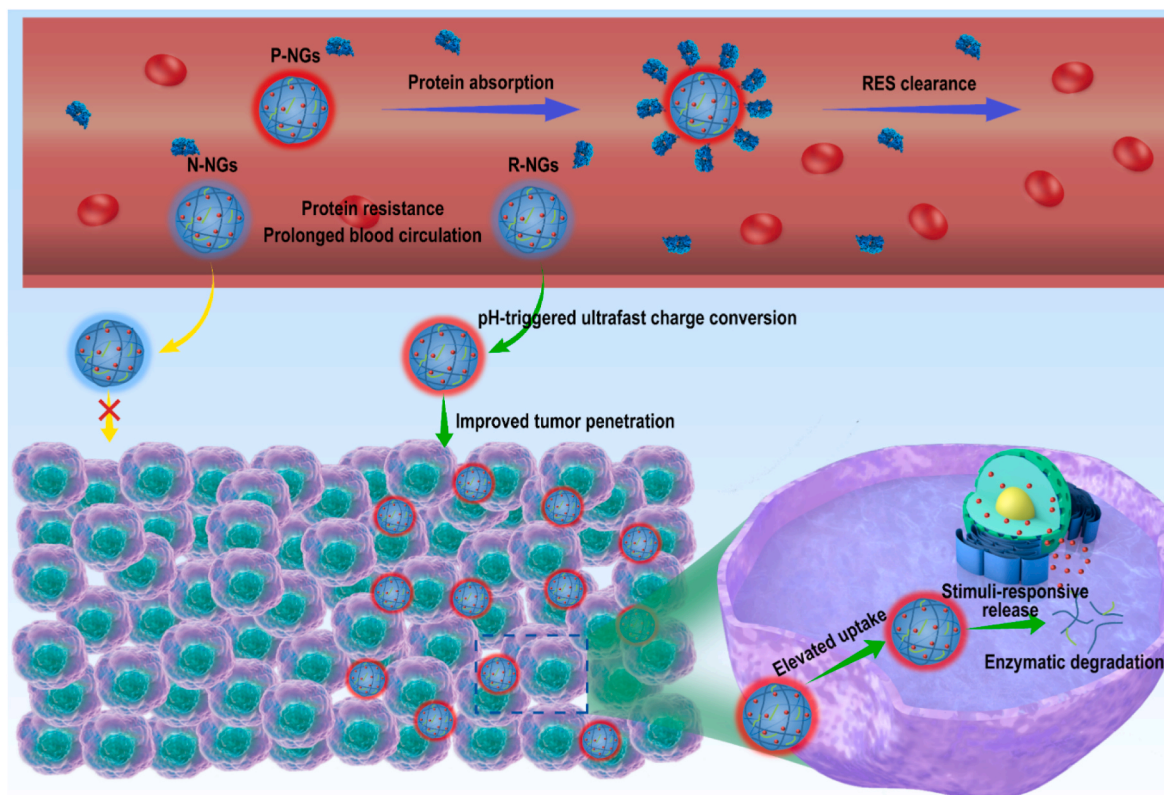
The prepared CH-PPy or CH-PPy-L NGs were purified by centrifugation (6000 rpm, 10 min), redispersion in 10 mL of water and dialysis in a bag with a molecular weight cut-off (MWCO) of 12000–14000 for 3 days against water (2 L, 6 times). Lastly, the CH-PPy NGs (1 mL) were treated with NaOH (1 mL) under different concentrations and molar ratios for 24 h to prepare a series of CH-PPy-OH NGs with different surface potentials (Table 1).

2.2. Preparation of FI-R-NGs and FI-N-NGs

The formed R-NGs or N-NGs (50 mg) dissolved in 2 mL DMSO were reacted with fluorescein isothiocyanate (FI, 10 mg, in 2 mL DMSO) under vigorous stirring in the dark. After 24 h, the solution was dialyzed using a dialysis membrane (MWCO = 12000–14000) and freeze-dried to obtain FI-R-NGs or FI-N-NGs. Furthermore, FI-R-NGs or FI-N-NGs (5 mg) and DOX (1 mg) were co-dissolved in 5 mL water under stirring for 24 h in the dark. Free DOX was removed by centrifugation (11000 rpm, 10 min) to obtain the FI-R-NGs/DOX or FI-N-NGs/DOX complexes.

2.3. *In vitro* cell culture and assays

A2780 cells (a human ovarian carcinoma cell line) were regularly cultured and passaged for cytocompatibility, cellular uptake, 3D tumor spheroid penetration, and anticancer activity assays of the developed charge-reversal NGs.



Scheme 1. Schematic illustration of drug delivery procedure of CH-PPy NGs (P-NGs), CH-PPy-OH-6 NGs (N-NGs) and CH-PPy-OH-4 NGs (R-NGs), and the use of R-NGs with prolonged blood circulation, improved tumor deep penetration, elevated cellular internalization, stimuli-responsive drug release and enzymatic degradation for augmented tumor chemotherapy. The definition of P-NGs, R-NGs, and N-NGs is shown in Table 1. The corona on the surface of NGs represents the surface charge (red for positive charge and blue for negative charge), not the core/shell structure of NGs.

Table 1

CH-PPy NGs (1 mL) treated with a series of NaOH solution (1 mL) under different concentrations and molar ratios.

Samples	$C_{\text{NGs}}(\text{mg/mL})/C_{\text{NaOH}}(\text{mg/mL})$	Molar ratio of $n_{\text{PPy}}/n_{\text{NaOH}}$
CH-PPy NGs (P-NGs)	–	–
CH-PPy-OH-1 NGs	5 : 2	1 : 1.25
CH-PPy-OH-2 NGs	5 : 4	1 : 2.5
CH-PPy-OH-3 NGs	1 : 2	1 : 6.25
CH-PPy-OH-4 NGs (R-NGs)	1 : 4	1 : 12.5
CH-PPy-OH-5 NGs	1 : 8	1 : 25
CH-PPy-OH-6 NGs (N-NGs)	1 : 20	1 : 62.5
CH-PPy-L-OH NGs	1.07 : 1	1 : 12.5

2.4. *In vivo* animal experiments

All animal experiments were approved by the Ethical Committee of Shanghai XinHua Hospital and also followed the policy of the National Ministry of Health. The charge-reversal NGs were subjected to pharmacokinetics, tumor accumulation, anticancer efficacy assays *in vivo*. See additional details in the Supplementary data.

3. Results and discussion

3.1. Synthesis and characterization of ultrafast charge-reversal CH-PPy-OH NGs

One effective approach to promote the active transportation of nanocarriers to tumor site is through the cationic charge-mediated endocytosis and adsorption-mediated transcytosis [42–44]. It is pivotal to design functional NGs with fast and effective cationic charge

transfer in the acidic tumor microenvironment (TME). To obtain ultrafast pH-triggered charge-reversal NGs with good biocompatibility, the CH-PPy polymers were first synthesized by a chemical oxidation polymerization method, followed by crosslinking with GA through an inverse miniemulsion method (Fig. 1a). Based on thermal gravimetric analysis (TGA), the CH-PPy polymers display a reduced weight loss at 200–450 °C (related to the degradation of CH) and further reduced weight loss at 450–800 °C (related to the degradation of PPy) when compared to CH (Fig. S1), suggesting that CH-PPy polymers have been successfully prepared. In the ^1H NMR spectra (Fig. 1b), the peaks at about 3.0 ppm (1) and 3.4–4.0 ppm (2–6) are assigned to the methylene and methylidene protons of CH, respectively, and the peak at around 7.7 ppm (7) is related to aromatic protons of Py ring. By NMR integration, the number of Py grafted to each CH unit was calculated to be 1.3. It should be noted that during the synthesis process, PPy homopolymer can be removed by the purification step of the centrifugation and ethanol washing, and the yield of CH-PPy can reach 63.5%. The prepared CH-PPy NGs (P-NGs) in dehydrated state exhibit an average diameter of 132.3 nm and uniform morphology, which were confirmed by transmission electron microscopy (TEM) imaging (Fig. 1c and Fig. S2). Moreover, through dynamic light scattering (DLS) measurement, the hydrodynamic diameter of P-NGs was determined to be 206.2 nm (PDI = 0.174) (Fig. S3), which is bigger than the size measured from TEM. This should be ascribed to the swelling behavior of P-NGs in aqueous solution. As demonstrated in the literature [45], the size of the P-NGs should be suitable for tumor accumulation and penetration.

The generated P-NGs were characterized by Fourier transform infrared (FTIR) spectroscopy (Fig. 1d). Compared to CH, the peaks at 1563 cm^{-1} and 1465 cm^{-1} are related to $\text{C}=\text{C}$ and $\text{C}-\text{N}$ asymmetric and symmetric stretching vibration of Py ring, respectively, and the peak at 747 cm^{-1} is from $-\text{NH}-$ bond for the CH-PPy polymers, revealing that

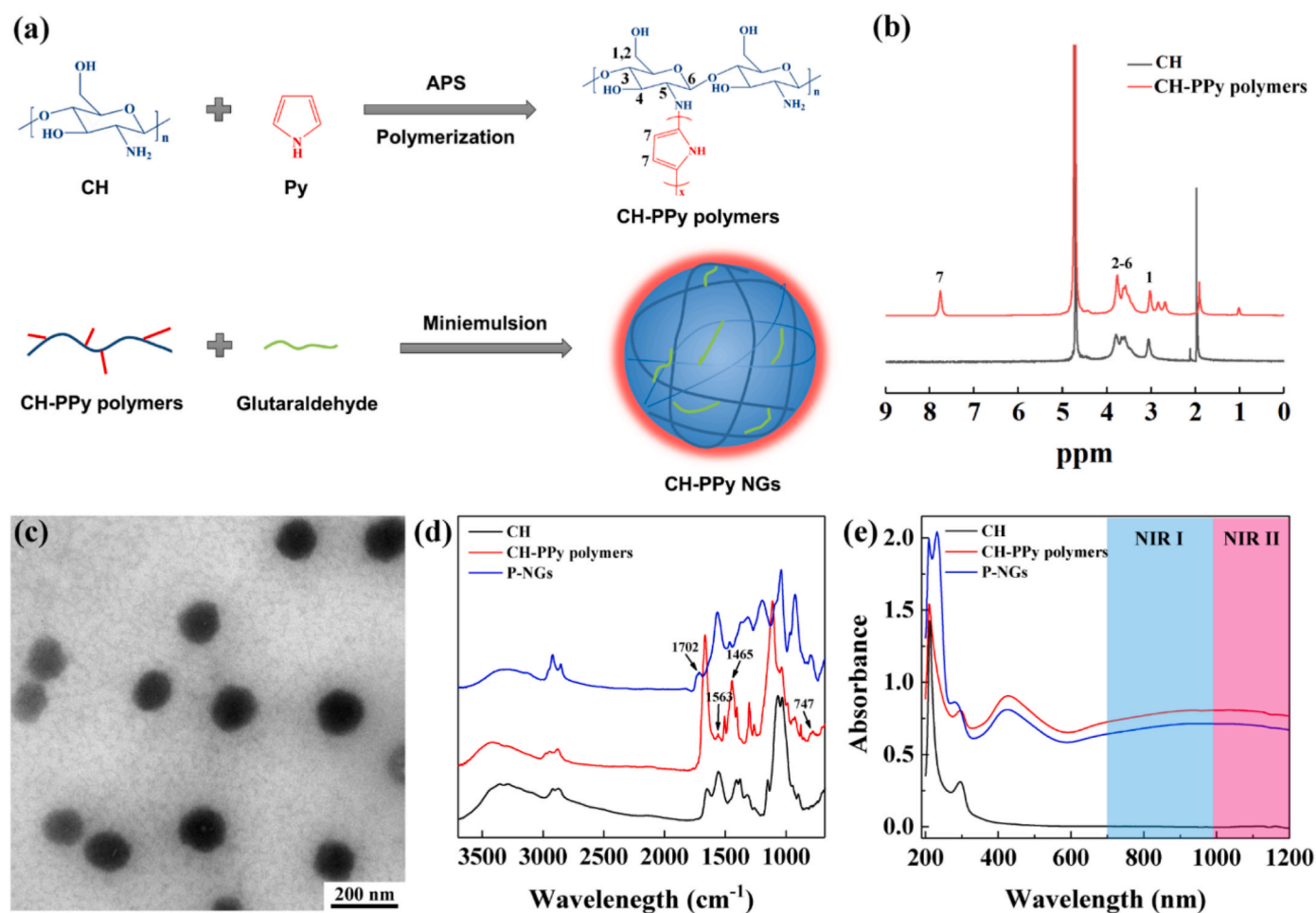


Fig. 1. (a) Schematic illustration of the preparation of the CH-PPy polymers and CH-PPy NGs (P-NGs). (b) ^1H NMR spectra of CH and CH-PPy polymers dispersed in D_2O with 2 vol% CD_3COOD . (c) TEM image of P-NGs. (d) FTIR spectra of CH, CH-PPy polymers and P-NGs. (e) UV-vis-NIR spectra of CH, CH-PPy polymers and P-NGs.

the Py has been grafted with CH successfully. Likewise, the new peak appearing at 1702 cm^{-1} for the P-NGs is attributed to the Schiff base group ($-\text{N}=\text{CH}-$), suggesting the success of the cross-linking reaction between amine groups of chitosan and aldehyde groups of GA. Furthermore, the optical property of CH-PPy NGs was checked by UV-vis-NIR spectrometry (Fig. 1e). Apparently, compared to CH, CH-PPy polymers and P-NGs possess the obviously enhanced absorption in the NIR I and II region from 700 to 1200 nm due to the grafted PPy. After that, the P-NGs were treated with NaOH solution under different concentrations and molar ratios for 24 h to obtain a series of CH-PPy-OH NGs (Table 1).

To obtain the suitable CH-PPy-OH NGs that can display pH-triggered charge conversion from negative to positive (Fig. 2a), the surface potentials of a series of CH-PPy-OH NGs were measured at both pH 7.4 and pH 6.5 which represent the physiological and TME conditions, respectively (Fig. 2b). The CH-PPy NGs (P-NGs) show positive charge at both pH 7.4 and pH 6.5, which is considered to be easily cleared by RES during the blood circulation. After treatment with a certain amount of NaOH solution, the NGs could be rendered with a negative charge due to the selective adsorption of OH^- on the Py rings (Fig. 2a), in agreement with the mechanism reported in the literature [46]. This may be because the introduction of oxygen atoms in CH-PPy-OH NGs renders OH^- near the solid-liquid interface rearranged in a different way named flop-down state. Clearly, the formed CH-PPy-OH-3 and CH-PPy-OH-4 NGs possess obvious charge conversion (negative to positive, R-NGs) from pH 7.4 to pH 6.5, attributing to the protonation of Py ring (Fig. 2b). Further, the

charge-reversal capacity of CH-PPy-OH-6 NGs (N-NGs) disappears after NaOH treatment, and the N-NGs remain negatively charged in-between pH 7.4 and pH 6.5. The surface potential changes of P-NGs and CH-PPy-OH-4 NGs (R-NGs) can be found in a broad pH range of 3–11 (Fig. S4). Next, the surface charge conversion of R-NGs was tracked (Fig. 2c). The ultrafast charge conversion of R-NGs from -11.3 mV to $+10.4\text{ mV}$ occurred after the solution pH was switched from pH 7.4 to 6.5, and this process only took about 10 s. The stability of charge conversion effect of R-NGs was detected at both pH 7.4 and pH 6.5 for a long time period (Fig. S5). The result reveals that the surface charges of R-NGs were maintained at around $+11.0\text{ mV}$ at pH 6.5 and -11.5 mV at pH 7.4 for as long as 15 h. Interestingly, the process of charge conversion of R-NGs is reversible (Fig. S6). Additionally, the long-term colloidal stability of R-NGs dispersed in phosphate buffer at both pH 7.4 and pH 6.5 was examined and confirmed by monitoring their hydrodynamic diameter changes at room temperature (Fig. S7). Clearly, the hydrodynamic diameter of the R-NGs does not have any appreciable changes after storage for at least 7 days.

Next, the universality of pH-triggered charge conversion of R-NGs with different PPy modification degrees was explored. The CH-PPy-L polymers were prepared and characterized by NMR (Fig. S8), where the number of Py grafted to each CH unit can be calculated to be 0.3, which is much lower than that for the CH-PPy polymers (1.3). This means that by varying the initial feeding ratio between the Py and CH, CH-PPy polymers with different PPy modification degrees can be obtained. At a lower Py/CH feeding ratio, a lower percentage of PPy

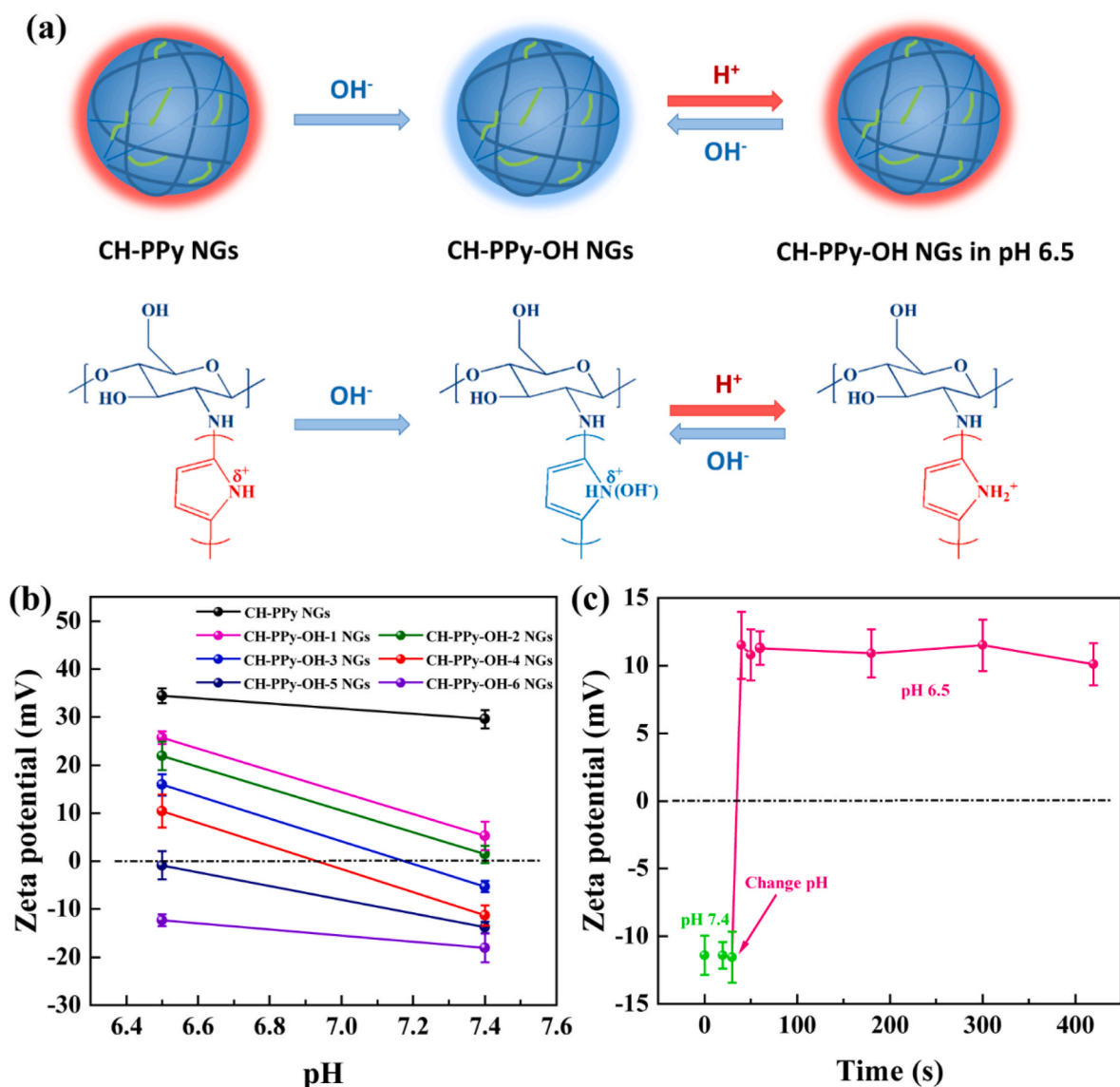


Fig. 2. (a) Schematic illustration of the facile preparation of CH-PPy-OH NGs and the pH-dependent ultrafast charge conversion between pH 7.4 and pH 6.5. (b) Zeta potentials of the CH-PPy-OH NGs after treatment with different NaOH concentrations and molar ratios at pH 7.4 and pH 6.5. (c) The time-dependent surface charge conversion of R-NGs after switching the solution pH from 7.4 to 6.5.

grafting can be achieved. Subsequently, the corresponding CH-PPy-L NGs and CH-PPy-L-OH NGs were synthesized and characterized. Encouragingly, the CH-PPy-L-OH NGs also display a pH-triggered charge conversion property (negative to positive) from pH 7.4 to pH 6.5 (Fig. S9). As a comparison, the surface potential change value of CH-PPy-L-OH NGs is relatively smaller than that of the R-NGs. Likewise, the NGs with a low PPy grafting or GA crosslinking degree exhibit a higher surface potential at pH 7.4 than those with a high PPy grafting or GA crosslinking degree, likely due to the relatively more residual amine groups of CH (Table S1). In any case, our data suggest that the developed approach is universal for the preparation of charge-reversal NGs based on the CH-PPy or CH-PPy-L polymers.

For the systemic administration of nanomedicines, it is necessary to endow the nanocarriers with the capacity of protein resistance to reduce RES clearance and prolong their blood circulation times. The protein resistance behavior of P-NGs, R-NGs and N-NGs was checked using bovine serum albumin (BSA) as a model protein under both pH 7.4 and pH 6.5 conditions to simulate blood and TME, respectively (Fig. 3a and b). As a quantitative comparison, the amount of BSA adsorbed onto the NGs was determined and calculated according to our previous work

[21]. It is demonstrated that the P-NGs have significantly higher protein adsorption at both pH 7.4 and pH 6.5 than both R-NGs and N-NGs ($p < 0.001$), owing to their rich surface positive charges. As expected, the R-NGs and N-NGs with negative surface charges display extremely low protein adsorption at pH 7.4 ($p > 0.05$). In contrast, an obviously higher protein adsorption was observed by R-NGs than by N-NGs at pH 6.5 ($p < 0.001$). This should be due to the fact that the charge conversion of R-NGs is triggered at pH 6.5 to be positive, activating the protein interaction. These results indicate that P-NGs with positive charges under both blood and TME conditions can easily induce protein adsorption through strong electrostatic interaction and can be rapidly cleared by RES. In contrast, both R-NGs and N-NGs with negative surface charges at the blood pH condition can be rendered with excellent protein resistance property, thus having prolonged blood circulation time. Most strikingly, the R-NGs with a charge-reversal property could be an ideal nanocarrier to have extended blood circulation time, and facilitate active transportation in the tumor site for enhanced penetration and intracellular uptake through electrostatic interactions.

For biomedical applications *in vivo*, the biodegradation of nanocarriers is extremely important to avoid the long-term toxicity. CH is a

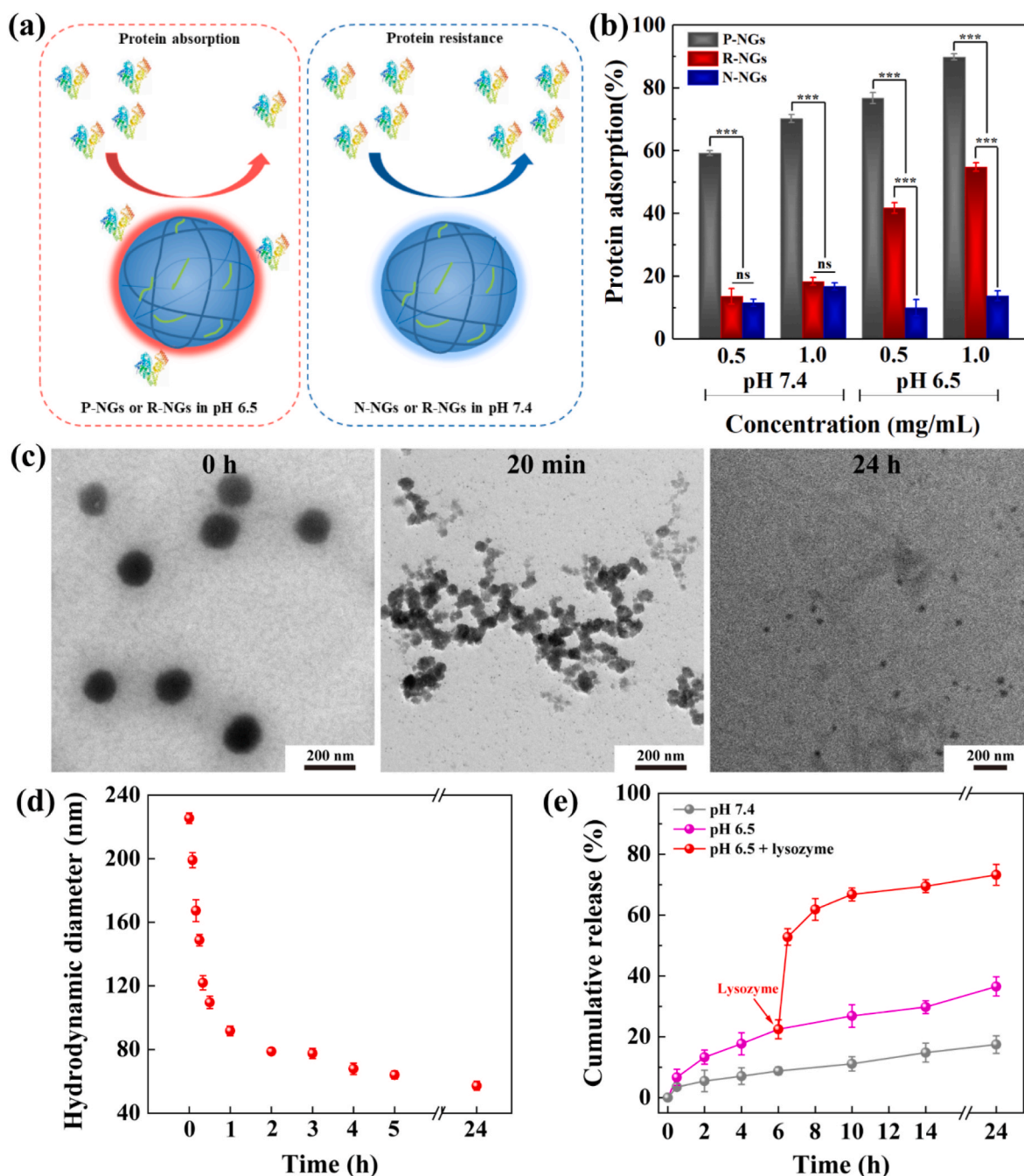


Fig. 3. (a) Schematic illustration of protein absorption and resistance of NGs. (b) Protein resistance assay of P-NGs, R-NGs and N-NGs with different concentrations at both pH 7.4 and pH 6.5. (c) TEM images and (d) size change of R-NGs at a lysozyme solution (pH 6.5) for different degradation times. (e) Cumulative release of DOX from R-NGs/DOX at pH 7.4 or pH 6.5 condition with/without lysozyme.

non-toxic, non-hemolytic and non-irritating biopolymer that is biodegradable through the enzymatic glycosidic linkage cleavage [47–49]. Next, the biodegradability of R-NGs was tested in the presence of lysozyme. Both TEM imaging and DLS results reveal that the R-NGs can be gradually degraded by lysozyme at pH 6.5 with the time (Fig. 3c and d). The initial fast degradation was observed during the first 20 min, followed by a slow degradation within 24 h. The enzyme-responsive degradation of R-NGs is likely to endow them with a controlled drug release behavior, and the degraded fragments are small enough to be metabolized by the kidney *in vivo* [50].

3.2. Drug encapsulation and release

The formed P-NGs, R-NGs and N-NGs were employed as nanocarriers to load DOX, and the DOX loading efficiency was measured (Table 2). It can be found that only around 26.21% loading efficiency is obtained for P-NGs/DOX due to the electrostatic repulsion between P-NGs and positively charged DOX·HCl. For comparison, the loading efficiencies of R-NGs/DOX and N-NGs/DOX are up to 87.58% and 89.63%, respectively, attributing to the electrostatic interaction between R-NGs/N-NGs and DOX·HCl. Hence, both R-NGs and N-NGs are suitable nanocarriers for DOX loading with a high efficiency.

Furthermore, the DOX release from the R-NGs/DOX was explored under different pH conditions in the presence or absence of lysozyme

Table 2
The DOX loading efficiency of P-NGs/DOX, R-NGs/DOX and N-NGs/DOX.

Samples	NGs concentration (mg/mL)	DOX concentration (mg/mL)	DOX loading efficiency (%)
P-NGs/DOX			26.21
R-NGs/DOX	5.0	1.0	87.58
N-NGs/DOX			89.63

(Fig. 3e). Clearly, at pH 7.4, the DOX release from R-NGs/DOX is slow and the cumulative release remains 17.45% after 1 day. For comparison, at pH 6.5, DOX can be quickly released from R-NGs/DOX and the cumulative release reaches about 36.53%. The pH-responsive release may be caused by the fact that the proton sponge effect appears between

cationic R-NGs and DOX·HCl under an acidic environment to facilitate fast DOX release through electrostatic repulsion between the NGs and DOX, in agreement with the literature [51,52]. This should be beneficial for inhibiting cancer cells, instead of normal tissues owing to the difference between tumor region (pH 6.5) and normal tissues (pH 7.4). Moreover, the DOX release from R-NGs/DOX in the presence of lysozyme at pH 6.5 is further dramatically promoted and the cumulative release reaches 73.22% due to the degradation of NGs. However, the DOX release from N-NGs/DOX is very slow at both pH 7.4 and 6.5 owing to their irreversible negative surface charge (Fig. S10). These results demonstrate that the R-NGs/DOX display pH/enzyme dual stimuli-responsive drug release performance.

3.3. Cytocompatibility and cellular internalization

Before the cell experiments, the colloidal stability of NGs dispersed in

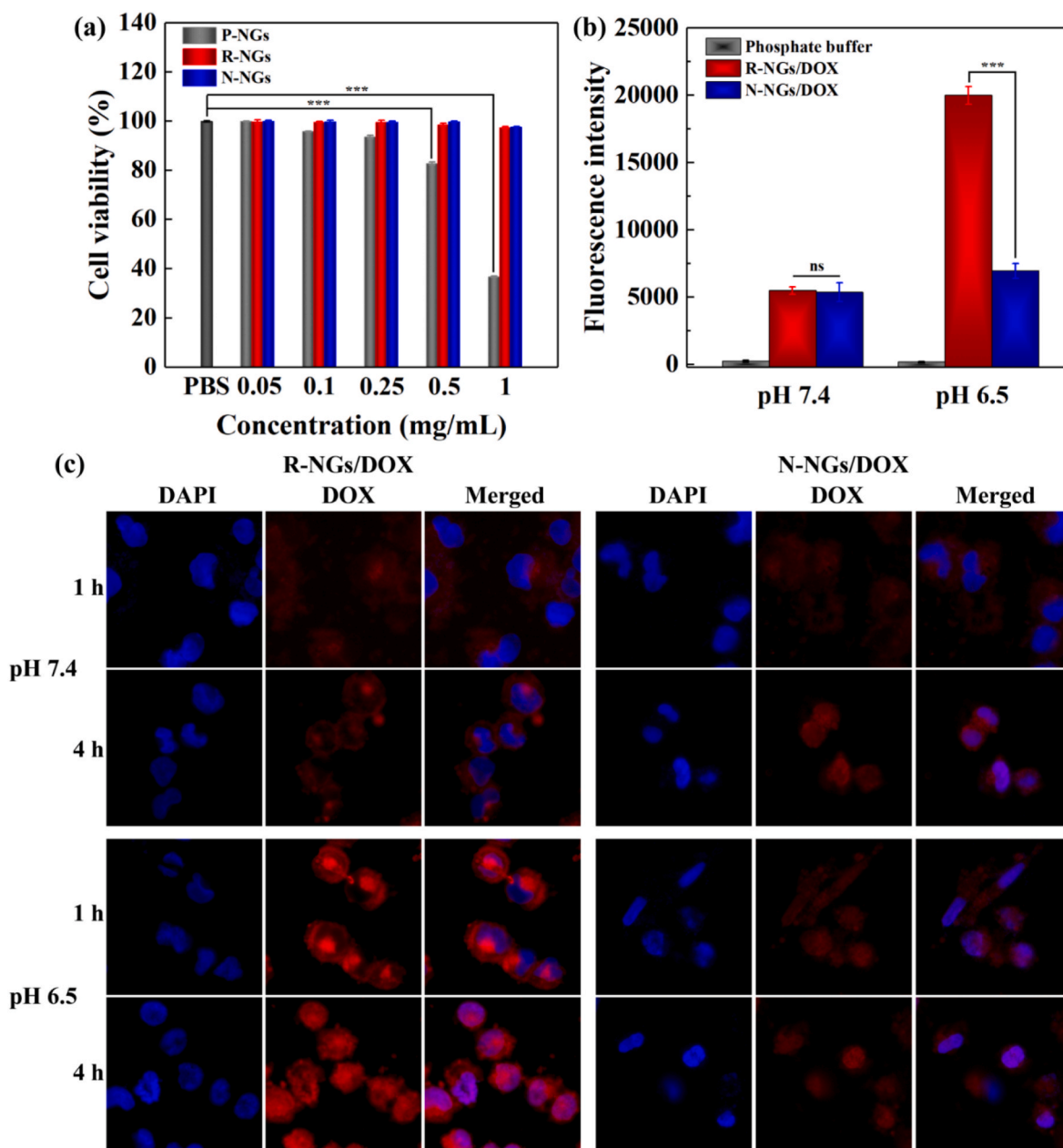


Fig. 4. (a) CCK-8 viability assay of A2780 cells treated with P-NGs, R-NGs and N-NGs with different concentrations for 24 h under regular culture medium (pH = 7.4). (b) Flow cytometric analysis of A2780 cells treated with R-NGs/DOX and N-NGs/DOX at both pH 7.4 and pH 6.5 medium for 4 h. (c) CLSM images of A2780 cells treated with R-NGs/DOX and N-NGs/DOX at both pH 7.4 and pH 6.5 medium for different time points, respectively ($\times 400$).

cell culture medium with serum at 37 °C was tested by DLS (Fig. S11). Clearly, both the R-NGs and N-NGs have stable hydrodynamic sizes and are colloidally stable in medium for at least 7 days. Next, the cytocompatibility of NGs was tested through Cell Counting Kit-8 (CCK-8) assay of the viability of A2780 cells (Fig. 4a). The viability of cells treated with P-NGs significantly decreases to 36.81% at the highest concentration of 1 mg/mL, indicating that the positively charged P-NGs present cytotoxicity. The P-NGs with a high surface potential may destroy the integrity of negatively charged cell membranes by strong electrostatic interaction to result in the leakage of cellular contents and cell death [53]. In contrast, the viability of cells treated with both R-NGs and N-NGs has no significant changes when compared to the PBS control, and can maintain above 97% at the highest concentration (1 mg/mL) tested. This indicates that both R-NGs and N-NGs show good cytocompatibility and may be used as promising and safe nanocarriers for biomedical applications.

To prove our hypothesis that the charge conversion leads to enhanced cellular internalization, the A2780 cells were incubated with R-NGs/DOX or N-NGs/DOX at both pH 7.4 and pH 6.5 medium for 4 h, followed by flow cytometry assay (Fig. 4b and Fig. S12). At pH 7.4 medium, the mean fluorescence in both R-NGs/DOX and N-NGs/DOX groups is low, and they do not show a significant difference ($p > 0.05$). Importantly, at pH 6.5 medium, the mean fluorescence in R-NGs/DOX group is obviously higher than that in N-NGs/DOX group ($p < 0.001$). These results suggest that the R-NGs/DOX exhibit a prominent advantage to facilitate enhanced cellular uptake due to their charge-reversal property at an acidic TME. The cationic R-NGs/DOX are able to elevate the affinity with cell membrane for enhanced cellular uptake, and this mechanism has been proven in the latest literature [32,33].

Furthermore, confocal laser scanning microscopy (CLSM) was performed to confirm the enhanced cellular internalization of R-NGs/DOX by A2780 cells at different pHs for 1 h and 4 h, respectively (Fig. 4c). Clearly, after 1 h of incubation, compared to other groups, the R-NGs/DOX can transport more DOX into A2780 cells at pH 6.5 owing to the enhanced cellular internalization. Moreover, the R-NGs/DOX efficiently deliver and release DOX into the cell nuclei at pH 6.5 after incubation for 4 h to improve anticancer activity (overlap of red and blue fluorescence), due to the pH-responsive drug release and proton sponge effect. Moreover, to visualize the cellular internalization of the NGs, FI-labelled NGs with the same labeling efficiency before and after DOX encapsulation were incubated with cells. CLSM imaging data (Fig. S13) reveal that cells incubated with the FI-R-NGs at pH 6.5 display the highest fluorescence intensity among cells treated with FI-R-NGs at pH 7.4 and FI-N-NGs at both pH 7.4 and pH 6.5. Additionally, the co-localization of the NGs (green fluorescence) and DOX is also shown in Fig. S14, which is consistent with the results shown in Fig. 4c and Fig. S13. These results imply that the charge-reversal property of R-NGs/DOX is effective to elevate their cellular uptake and internalization, promoting drug release to cell nucleus for optimal anticancer therapy.

3.4. Penetration of 3D cell spheroids and anticancer efficacy *in vitro*

The concept that nanocarriers penetrate into the tumor region through tissue gaps is an important rationale for cancer nanomedicine. Thus, several innovative strategies related to the ECM degradation using hyaluronidase or size-switching (large to small) by a specific stimuli have been explored to reduce penetration hindrance and improve nanocarriers transportation [25,39]. However, the latest discovery demonstrates that most of the nanocarriers penetrate and enter into solid tumors by active transportation of transcytosis rather than passive diffusion through tissue gaps [31], which questions and challenges the current rationale [4,54]. Likewise, another latest work verifies that the active transportation of transcytosis can be achieved effectively by the cationization of nanocarriers to facilitate the deep tumor penetration across multiple cell layers to reach the distal tumor region [32,33].

The penetration ability and active transportation of R-NGs/DOX

within 3D A2780 multicellular spheroids tumor model (MSTM), which could better simulate the TME, was investigated (Fig. 5a–c). It is clear that the MSTM treated with the R-NGs/DOX and N-NGs/DOX displays increased red fluorescence of DOX with the incubation time, and the DOX fluorescence diffuses gradually from the periphery to the interior. Although the sizes of R-NGs/DOX and N-NGs/DOX are similar, the DOX fluorescence intensity and penetration depth of MSTM treated with the R-NGs/DOX are significantly higher than those treated with the N-NGs/DOX at the same incubation time points ($p < 0.01$). To further validate that the rapid penetration is based on the active transportation of transcytosis, the MSTM was pretreated with the endocytosis inhibitor genistein. As expected, the R-NGs/DOX are restricted to the peripheral of MSTM after treated with the genistein, in agreement with the literature [32]. These results indicate that pH-responsive ultrafast charge conversion of R-NGs/DOX may be beneficial for them to have improved tumor penetration through active transportation.

The viability of the A2780 cells treated with the R-NGs/DOX and N-NGs/DOX at pH 7.4 and pH 6.5 medium was measured by CCK-8 assay to evaluate their anticancer efficacy (Fig. 5d and e). At pH 7.4, the anticancer efficacy of both R-NGs/DOX and N-NGs/DOX shows a DOX concentration-dependent increasing trend, and their efficacies show no significant difference ($p > 0.05$). This is because the negative surface charge of R-NGs/DOX and N-NGs/DOX at pH 7.4 limits their uptake by cancer cells due to the electrostatic charge repulsion, and the DOX release at pH 7.4 is relatively slow. Strikingly, cells treated with the R-NGs/DOX display a much lower viability than those treated with the N-NGs/DOX at pH 6.5 ($p < 0.01$) at the same DOX concentrations. Moreover, the half maximal inhibitory concentrations (IC₅₀s) of all samples were calculated and compared (Table S2). At pH 6.5, the IC₅₀ follows the order of N-NGs/DOX (4.80 μg/mL) > R-NGs/DOX (1.81 μg/mL) > free DOX (0.88 μg/mL). Notably, the R-NGs/DOX display a 2.6-times lower IC₅₀ value at pH 6.5 than N-NGs/DOX. Furthermore, the cell nuclei staining with Hoechst 33342 was performed to confirm the cell apoptosis (Fig. S15). The typical apoptotic morphologic change of hyperchromatic nuclei (punctate blue fluorescence) occurred in the cells treated with both R-NGs/DOX and N-NGs/DOX, suggesting that DOX can induce cell apoptosis. As expected, the cells treated with R-NGs/DOX display a more significant chromatic condensation than those treated with N-NGs/DOX. These results suggest that the R-NGs/DOX exhibit a superior anticancer efficacy because of the enhanced cellular internalization and facilitated drug release at an acidic TME.

3.5. Pharmacokinetics and tumor accumulation *in vivo*

Pharmacokinetics of the R-NGs/DOX was next investigated. After intravenous injection, the blood DOX concentration at different time points was determined (Fig. 6a). The R-NGs/DOX and N-NGs/DOX show a relatively long half-decay time ($t_{1/2}$) of 6.03 h and 6.20 h, respectively, which is 21.5 and 22.1 times longer than that of free DOX (0.28 h). This result reveals that the R-NGs/DOX and N-NGs/DOX with quite good protein resistance possess reduced RES clearance and prolonged blood circulation time due to their negative surface charges, which is beneficial for the drug nanocarriers to be accumulated within tumors.

The time-dependent tumor accumulation of DOX was further measured after intravenous injection of R-NGs/DOX or N-NGs/DOX (Fig. 6b). At 24 h postinjection, the tumor accumulation of DOX for both R-NGs/DOX and N-NGs/DOX reaches a peak value, and then decreases gradually due to the metabolic process. More significantly, at 24 h postinjection, the tumor DOX accumulation in R-NGs/DOX group is 2.2 times higher than that in N-NGs/DOX group ($p < 0.001$), and at the same time points, the tumor DOX accumulation in R-NGs/DOX group is much higher than that in N-NGs/DOX group. Encouragingly, through quantification, about 4.7% of DOX in the injected R-NGs/DOX accumulated in tumors at 24 h postinjection, obviously higher than that in the injected N-NGs/DOX (1.9%) and many other nanocarriers reported elsewhere (less than 1%) [4]. This should be attributed to the synergistic design of

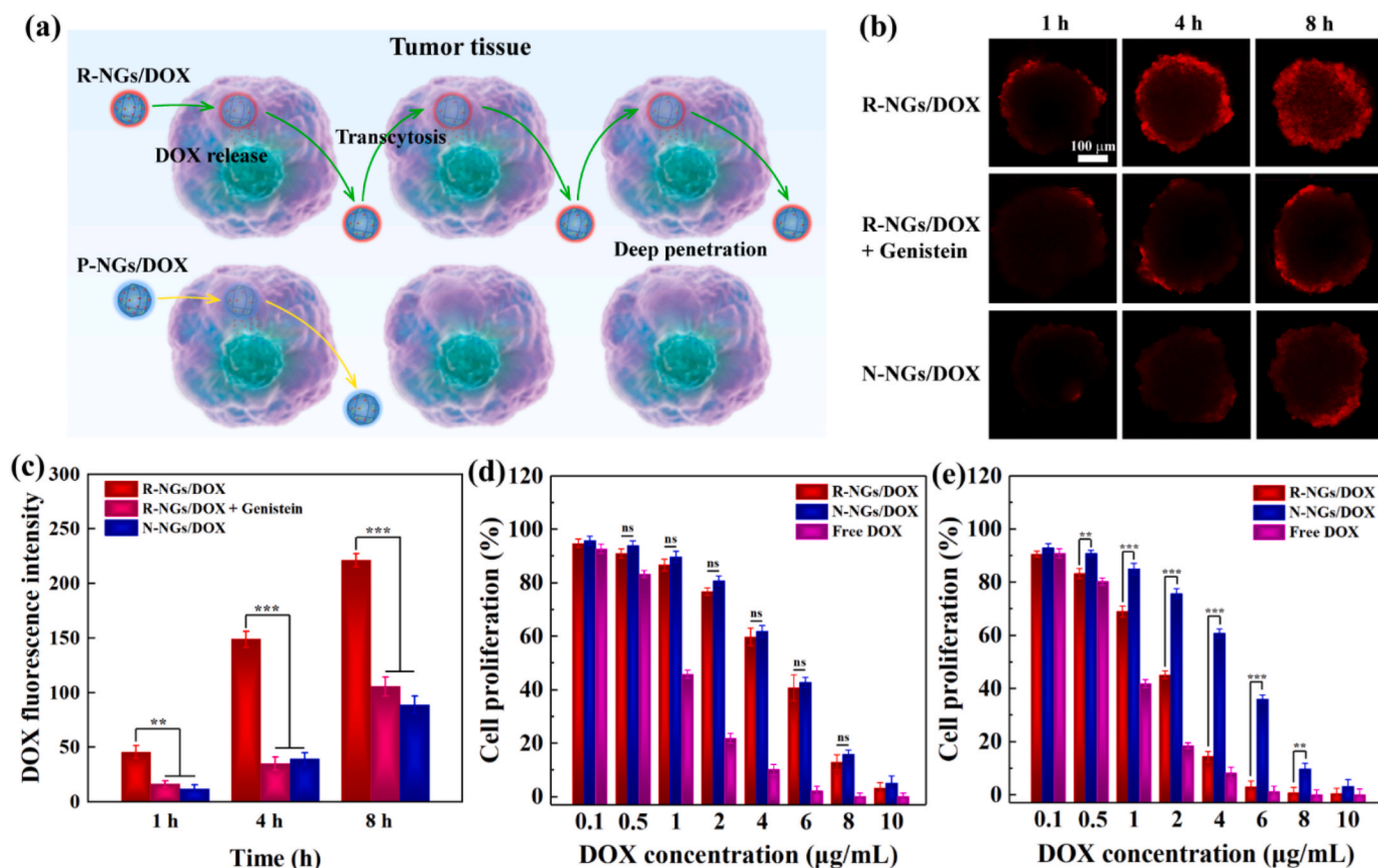


Fig. 5. (a) Schematic illustration of transcytosis of R-NGs for deep tumor penetration and drug release throughout the tumor. (b) CLSM images and (c) corresponding fluorescence intensity of A2780 MSTM treated with the R-NGs/DOX (with or without pretreatment of the endocytosis inhibitor genistein) and N-NGs/DOX for 1, 4, and 8 h, respectively. CCK8 proliferation assay of A2780 cells treated with free DOX, R-NGs/DOX and N-NGs/DOX with different DOX concentrations at (d) pH 7.4 and (e) pH 6.5 for 24 h, respectively.

NG system to have reduced RES clearance, prolonged blood circulation, improved tumor penetration and elevated cellular internalization.

3.6. Antitumor efficacy *in vivo*

To validate the augmented antitumor efficacy of R-NGs/DOX *in vivo*, the tumor volume change and survival rate were monitored in saline, R-NGs/DOX, N-NGs/DOX and free DOX groups, respectively after intravenous (i.v.) injection (Fig. 6c and d). In Fig. 6c and Fig. S16, the relative tumor volume in R-NGs/DOX group is the smallest at 21 days post treatment when compared with other groups. The tumor growth inhibitory effect in R-NGs/DOX group is significantly higher than that in N-NGs/DOX ($p < 0.001$) and free DOX ($p < 0.01$) groups. These results indicate that the R-NGs/DOX can indeed dramatically improve antitumor activity through the optimized delivery with reduced RES clearance, prolonged blood circulation, improved tumor penetration, elevated cellular internalization and stimuli-responsive drug release. In addition, the survival rates of mice in different groups were measured during 60 days to further investigate the antitumor efficacy (Fig. 6d). After 60 days, the mice in saline group are all dead, while the survival rate in the R-NGs/DOX group reaches 80%, much higher than that in the N-NGs/DOX group (20%) and free DOX group (40%). These results indicate that the R-NGs/DOX display the best tumor inhibit effect and can sufficiently prolong the survival life-span of mice.

Moreover, the antitumor efficacy of each group *in vivo* was further evaluated through TUNEL staining of tumor sections after different treatments (Fig. 6e, g). In comparison with the saline group that exhibits barely apoptotic cells (green fluorescence), a large number of apoptotic cells were observed in the R-NGs/DOX group, which is higher than in the

N-NGs/DOX and free DOX groups. Corresponding apoptosis rate analysis of each group shows that the tumor cell apoptosis rate follows the order of R-NGs/DOX (56.4%) > free DOX (29.7%) > N-NGs/DOX (21.4%) > saline (8.9%) (Fig. 6e). These results again demonstrate the excellent antitumor efficacy of R-NGs/DOX *in vivo* due to their owned multiple advantages.

3.7. Systemic toxicity and biodistribution

The toxicity and side effects *in vivo* of the R-NGs/DOX were evaluated by body weight change of mice, H&E staining of organs, and blood biochemistry. Body weights of the tumor-bearing mice were measured after different treatments (Fig. 6f). Clearly, the body weight in the free DOX group shows an obvious reduction compared to the other groups ($p < 0.01$), suggesting that free DOX exhibits side effects after systemic delivery. In contrast, there are no significant difference in the body weight change for all the other groups of R-NGs/DOX, N-NGs/DOX and saline, revealing that both R-NGs and N-NGs as nanocarriers can reduce the side effects of DOX *in vivo*. Moreover, H&E staining of the major organs of mice (heart, liver, spleen, lung and kidney) reveals that these organs in the groups of R-NGs/DOX, N-NGs/DOX and saline do not show any necrotic region (Fig. S17). Furthermore, the toxicity and side effects were detected by serum indicators of heart, liver and kidney function. The major blood biochemistry parameters, including lactate dehydrogenase (LDH), alanine aminotransferase (ALT), aspartate aminotransferase (AST), creatine kinase (CK), and CK-muscle/brain (CK-MB) were recorded in different groups (Fig. S18). These parameters in R-NGs/DOX and N-NGs/DOX groups are obviously higher than those in the free DOX group. These results illustrate that the developed NGs as nanocarriers

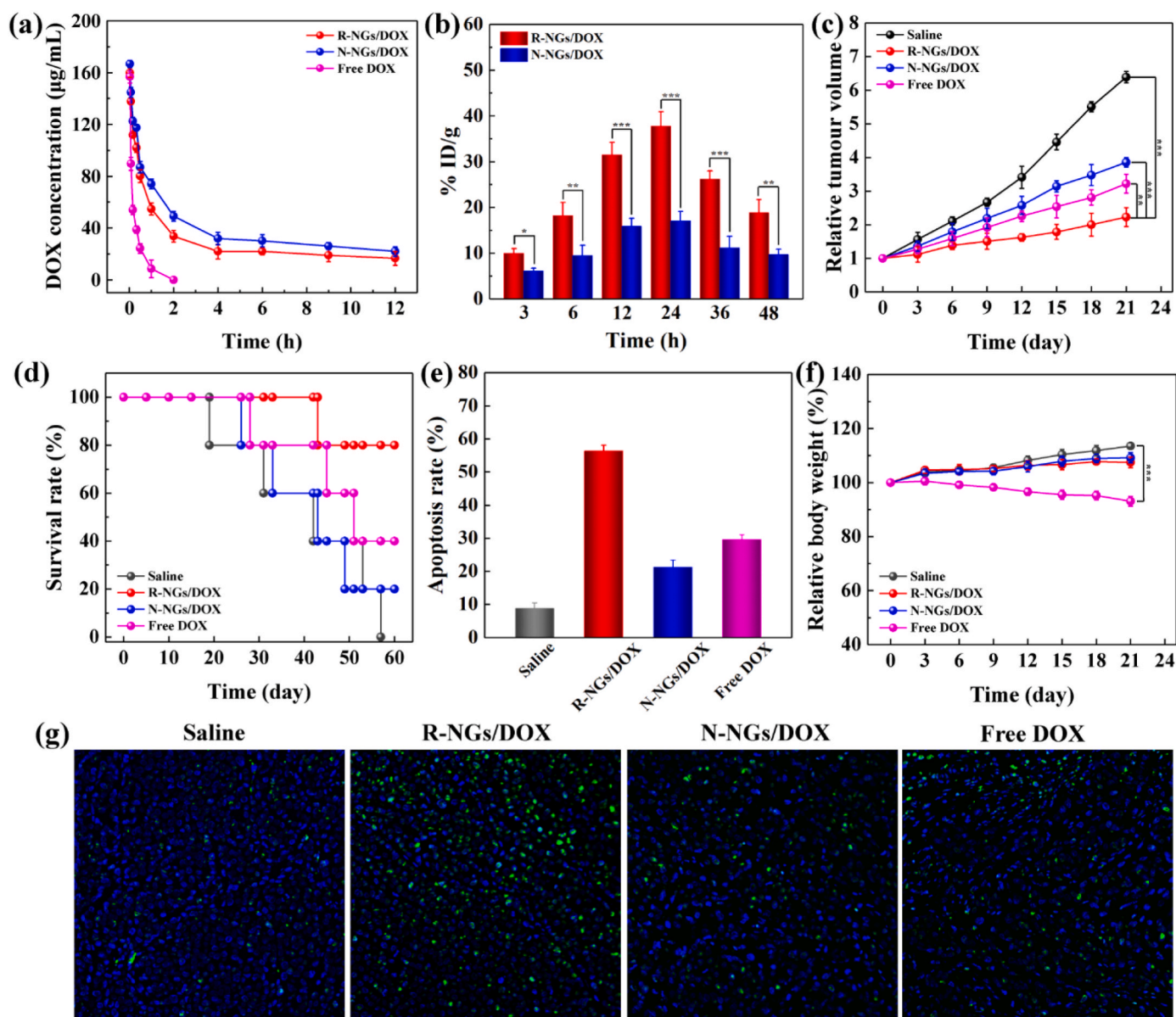


Fig. 6. (a) Pharmacokinetics of DOX after i.v. injection of R-NGs/DOX, N-NGs/DOX and free DOX in the healthy mice. (b) The accumulated DOX amount in tumors after i.v. injection of R-NGs/DOX and N-NGs/DOX in mice bearing A2780 xenografted tumors for different time periods. (c) Relative tumor volume, and (d) survival rate of mice bearing A2780 xenografted tumors as a function of time post i.v. injection of saline, R-NGs/DOX, N-NGs/DOX and free DOX ([DOX] = 5 mg/kg, 0.2 mL saline for each DOX-related group and for each mouse). (e) Quantitative analysis of the apoptosis rate of tumor cells in different treatment groups. (f) Body weight change of mice bearing A2780 xenografted tumors in different groups. (g) TUNEL staining of tumor sections in different groups ($\times 100$).

can protect the heart, liver and kidney function of mice, avoiding multiple organ failure and side effects.

Finally, the biodistribution and metabolic pathway of R-NGs/DOX *in vivo* were tracked by DOX measurement in major organs of mice after i.v. injection for different time periods (Fig. S19). Apparently, the DOX content was gradually accumulated in the liver and spleen at 24 h postinjection, and then metabolized after 24 h, revealing that the R-NGs/DOX *in vivo* can be cleared by the reticuloendothelial system organs.

4. Conclusion

In summary, we developed a facile method to prepare a self-adaptive ultrafast charge-reversible CH-PPy NG system to simultaneously prolong blood circulation and improve tumor penetration and intracellular uptake for augmented ovarian carcinoma chemotherapy. Through the

grafting of PPy with CH, biodegradable CH-PPy NGs with an average diameter of 132.3 nm were able to be synthesized and then optimized to have an ultrafast charge-reversal property after fine treatment with an alkaline solution. The formed R-NGs with a surface negative charge (-11.3 mV) under a physiological pH condition display good cytocompatibility, high anticancer drug DOX loading efficiency, excellent protein resistance and prolonged blood circulation time. Upon tumor site delivery, the DOX-loaded R-NGs are able to fast switch their surface charge to be positive (10.4 mV) in response to TME by rapid protonation of Py ring for improved tumor penetration, intracellular uptake, and responsive DOX release. Moreover, the ultrafast charge reversal R-NGs may also be modified with targeting ligands to achieve specific targeting of a particular cancer type for improved cancer therapeutics. With these excellent properties owned, the designed R-NGs can achieve significantly augmented chemotherapy of ovarian carcinoma with low side effects *in vivo*. The NGs possessing the strong absorption in the NIR

region may also be used for photoacoustic imaging and photothermal therapy. The designed CH-PPy NG system with a self-adaptive charge-reversal property may be developed as an intelligent nanomedicine for augmented therapy of different tumor types.

CRediT authorship contribution statement

Xin Li: Methodology, Software, Data curation, Writing – original draft. **Helin Li:** Data curation, Formal analysis, Writing – original draft. **Changchang Zhang:** Methodology, Software, Data curation. **Andrij Pich:** Supervision, Resources, Funding acquisition, Writing – review & editing. **Lingxi Xing:** Supervision, Resources, Funding acquisition, Writing – review & editing. **Xiangyang Shi:** Conceptualization, Supervision, Resources, Funding acquisition, Project administration, Writing – review & editing.

Declaration of competing interest

There are no conflicts of interest to declare.

Acknowledgements

This research was financially supported by the Sino-German Center for Research Promotion (GZ1505), National Natural Science Foundation of China (81801704 and 81761148028), the Science and Technology Commission of Shanghai Municipality (19XD1400100), Shanghai Sailing Program (18YF1415300), and the China Scholarship Council (for X. Li). X. Shi also thanks the support by FCT-Fundação para a Ciência e a Tecnologia through the CQM Base Fund - UIDB/00674/2020, and Programmatic Fund - UIDP/00674/2020, and by ARDITI-Agência Regional para o Desenvolvimento da Investigação Tecnologia e Inovação, through the project M1420-01-0145-FEDER-000005 - Centro de Química da Madeira - CQM+ (Madeira 14-20 Program).

Appendix A. Supplementary data

Supplementary data to this article can be found online at <https://doi.org/10.1016/j.bioactmat.2021.03.021>.

References

- [1] M.P. Stewart, A. Sharei, X.Y. Ding, G. Sahay, R. Langer, K.F. Jensen, In vitro and ex vivo strategies for intracellular delivery, *Nature* 538 (2016) 183–192.
- [2] Z.M. Zhao, A. Ukidve, Y.S. Gao, J. Kim, S. Mitragotri, Erythrocyte leveraged chemotherapy (ELeCt): nanoparticle assembly on erythrocyte surface to combat lung metastasis, *Sci. Adv.* 5 (2019), eaax9250.
- [3] G. Hannon, J. Lysaght, N.J. Liptrott, A. Prina-Mello, Immunotoxicity considerations for next generation cancer nanomedicines, *Adv. Sci.* 6 (2019) 1900133.
- [4] S. Wilhelm, A.J. Tavares, Q. Dai, S. Ohta, J. Audet, H.F. Dvorak, W.C.W. Chan, Analysis of nanoparticle delivery to tumours, *Nat. Rev. Mater.* 1 (2016) 16014.
- [5] J.L. Shen, J. Wolfram, M. Ferrari, H.F. Shen, Taking the vehicle out of drug delivery, *Mater. Today* 20 (2017) 95–97.
- [6] P.P. Adisheshaiah, R.M. Crist, S.S. Hook, S.E. McNeil, Nanomedicine strategies to overcome the pathophysiological barriers of pancreatic cancer, *Nat. Rev. Clin. Oncol.* 13 (2016) 750–765.
- [7] Y.S. Youn, Y.H. Bae, Perspectives on the past, present, and future of cancer nanomedicine, *Adv. Drug Deliv. Rev.* 130 (2018) 3–11.
- [8] N.T. Trac, E.J. Chung, Peptide-based targeting of immunosuppressive cells in cancer, *Bioact. Mater.* 5 (2020) 92–101.
- [9] J.d. Neves, R.S. Arzib, A. Sosnik, Molecular and cellular cues governing nanomaterial-mucosae interactions: from nanomedicine to nanotoxicology, *Chem. Soc. Rev.* 49 (2020) 5058–5100.
- [10] J. Fang, W. Islam, H. Maeda, Exploiting the dynamics of the EPR effect and strategies to improve the therapeutic effects of nanomedicines by using EPR effect enhancers, *Adv. Drug Deliv. Rev.* 157 (2020) 142–160.
- [11] Y. Hao, Y.W. Chen, X.L. He, F. Yang, R.X. Han, C.L. Yang, W. Li, Z.Y. Qian, Near-infrared responsive 5-fluorouracil and indocyanine green loaded MPEG-PCL nanoparticle integrated with dissolvable microneedle for skin cancer therapy, *Bioact. Mater.* 5 (2020) 542–552.
- [12] X. Li, S.Y. Lu, Z.G. Xiong, Y. Hui, D. Ma, W.Q. Lou, C. Peng, M.W. Shen, X.Y. Shi, Light-addressable nanoclusters of ultrasmall iron oxide nanoparticles for enhanced and dynamic magnetic resonance imaging of arthritis, *Adv. Sci.* 6 (2019) 1901800.
- [13] J.J. Chen, J.X. Ding, Y.C. Wang, J.J. Cheng, S.X. Ji, X.L. Zhuang, X.S. Chen, Sequentially responsive shell-stacked nanoparticles for deep penetration into solid tumors, *Adv. Mater.* 29 (2017) 1701170.
- [14] L.X. Xing, X. Li, Z.H. Xing, F. Li, M.W. Shen, H. Wang, X.Y. Shi, L.F. Du, Silica/gold nanoplatform combined with a thermosensitive gel for imaging-guided interventional therapy in PDX of pancreatic cancer, *Chem. Eng. J.* 382 (2020) 122949.
- [15] D. Ma, M.H. Shi, X. Li, J.L. Zhang, Y. Fan, K. Sun, T.T. Jiang, C. Peng, X.Y. Shi, Redox-sensitive clustered ultrasmall iron oxide nanoparticles for switchable T-2/T-1-weighted magnetic resonance imaging applications, *Bioconjugate Chem.* 31 (2020) 352–359.
- [16] M.X. Yu, J. Zheng, Clearance pathways and tumor targeting of imaging nanoparticles, *ACS Nano* 9 (2015) 6655–6674.
- [17] M.J. Ernsting, M. Murakami, A. Roy, S.D. Li, Factors controlling the pharmacokinetics, biodistribution and intratumoral penetration of nanoparticles, *J. Contr. Release* 172 (2013) 782–794.
- [18] X. Li, L.X. Xing, K.L. Zheng, P. Wei, L.F. Du, M.W. Shen, X.Y. Shi, Formation of gold nanostar-coated hollow mesoporous silica for tumor multimodality imaging and photothermal therapy, *ACS Appl. Mater. Interfaces* 9 (2017) 5817–5827.
- [19] L.D. Blackman, P.A. Gunatillake, P. Cass, K.E.S. Locoock, An introduction to zwitterionic polymer behavior and applications in solution and at surfaces, *Chem. Soc. Rev.* 48 (2019) 757–770.
- [20] X. Li, Z.G. Xiong, X.Y. Xu, Y. Luo, C. Peng, M.W. Shen, X.Y. Shi, ^{99m}Tc-labeled multifunctional low-generation dendrimer-entrapped gold nanoparticles for targeted SPECT/CT dual-mode imaging of tumors, *ACS Appl. Mater. Interfaces* 8 (2016) 19883–19891.
- [21] Z.J. Xiong, Y. Wang, J.Y. Zhu, X. Li, Y. He, J. Qu, M.W. Shen, J.D. Xia, X.Y. Shi, Dendrimers meet zwitterions: development of a unique antifouling nanoplatform for enhanced blood pool, lymph node and tumor CT imaging, *Nanoscale* 9 (2017) 12295–12301.
- [22] F. Zhao, Y. Zhao, Y. Liu, X.L. Chang, C.Y. Chen, Y.L. Zhao, Cellular uptake, intracellular trafficking, and cytotoxicity of nanomaterials, *Small* 7 (2011) 1322–1337.
- [23] S. Wang, L. Zhang, C.H. Dong, L. Su, H.J. Wang, J. Chang, Smart pH-responsive upconversion nanoparticles for enhanced tumor cellular internalization and near-infrared light-triggered photodynamic therapy, *Chem. Commun.* 51 (2015) 406–408.
- [24] G.B. Kim, V. Aragon-Sanabria, L. Randolph, H.L. Jiang, J.A. Reynolds, B.S. Webb, A. Madhankumar, X.J. Lian, J.R. Connor, J. Yang, C. Dong, High-affinity mutant Interleukin-13 targeted CAR T cells enhance delivery of clickable biodegradable fluorescent nanoparticles to glioblastoma, *Bioact. Mater.* 5 (2020) 624–635.
- [25] T.D. McKee, P. Grandi, W. Mok, G. Alexandrakis, N. Insin, J.P. Zimmer, M. G. Bawendi, Y. Boucher, X.O. Breakefield, R.K. Jain, Degradation of fibrillar collagen in a human melanoma xenograft improves the efficacy of an oncolytic herpes simplex virus vector, *Cancer Res.* 66 (2006) 2509–2513.
- [26] R.K. Jain, T. Stylianopoulos, Delivering nanomedicine to solid tumors, *Nat. Rev. Clin. Oncol.* 7 (2010) 653–664.
- [27] A. Jablonska-Trypuc, M. Matejczyk, S. Rosochacki, Matrix metalloproteinases (MMPs), the main extracellular matrix (ECM) enzymes in collagen degradation, as a target for anticancer drugs, *J. Enzym. Inhib. Med. Chem.* 31 (2016) 177–183.
- [28] D. Ling, W. Park, S.J. Park, Y. Lu, K.S. Kim, M.J. Hackett, B.H. Kim, H. Yim, Y. S. Jeon, K. Na, T. Hyeon, Multifunctional tumor pH-sensitive self-assembled nanoparticles for bimodal imaging and treatment of resistant heterogeneous tumors, *J. Am. Chem. Soc.* 136 (2014) 5647–5655.
- [29] S. Wang, P. Huang, X.Y. Chen, Hierarchical targeting strategy for enhanced tumor tissue accumulation/retention and cellular internalization, *Adv. Mater.* 28 (2016) 7340–7364.
- [30] L.Z. Feng, Z.L. Dong, D.L. Tao, Y.C. Zhang, Z. Liu, The acidic tumor microenvironment: a target for smart cancer nano-theranostics, *Natl. Sci. Rev.* 5 (2018) 269–286.
- [31] S. Sindhvani, A.M. Syed, J. Ngai, B.R. Kingston, L. Maiorino, J. Rothschild, P. MacMillan, Y.W. Zhang, N.U. Rajesh, T. Hoang, J.L.Y. Wu, S. Wilhelm, A. Zilman, S. Gadde, A. Sulaiman, B. Ouyang, Z. Lin, L.S. Wang, M. Egeblad, W.C. W. Chan, The entry of nanoparticles into solid tumours, *Nat. Mater.* 19 (2020) 566–575.
- [32] Q. Zhou, S.Q. Shao, J.Q. Wang, C.H. Xu, J.J. Xiang, Y. Piao, Z.X. Zhou, Q.S. Yu, J. B. Tang, X.R. Liu, Z.H. Gan, R. Mo, Z. Gu, Y.Q. Shen, Enzyme-activatable polymer-drug conjugate augments tumour penetration and treatment efficacy, *Nat. Nanotechnol.* 14 (2019) 799–809.
- [33] G.W. Wang, Z.X. Zhou, Z.H. Zhao, Q.Y. Li, Y.L. Wu, S. Yan, Y.Q. Shen, P.T. Huang, Enzyme-triggered transcytosis of dendrimer-drug conjugate for deep penetration into pancreatic tumors, *ACS Nano* 14 (2020) 4890–4904.
- [34] S. Pandit, D. Dutta, S.M. Nie, Active transcytosis and new opportunities for cancer nanomedicine, *Nat. Mater.* 19 (2020) 478–480.
- [35] J. Liu, S. Iqbal, X.J. Du, Y.Y. Yuan, X.Z. Yang, H.J. Li, J. Wang, Ultrafast charge-conversional nanocarrier for tumor-acidity-activated targeted drug delivery, *Biomater. Sci.* 6 (2018) 350–355.
- [36] J.Z. Zhu, T.T. Xiao, J.L. Zhang, H.L. Che, Y.X. Shi, X.Y. Shi, J.C.M. van Hest, Surface-charge-switchable nanoclusters for magnetic resonance imaging-guided and glutathione depletion-enhanced photodynamic therapy, *ACS Nano* 14 (2020) 11225–11237.
- [37] H.J. Li, J. Liu, Y.L. Luo, S.B. Chen, R. Liu, J.Z. Du, J. Wang, Intratumor performance and therapeutic efficacy of PAMAM dendrimers carried by clustered nanoparticles, *Nano Lett.* 19 (2019) 8947–8955.

- [38] C.Y. Sun, S. Shen, C.F. Xu, H.J. Li, Y. Liu, Z.T. Cao, X.Z. Yang, J.X. Xia, J. Wang, Tumor acidity-sensitive polymeric vector for active targeted siRNA delivery, *J. Am. Chem. Soc.* 137 (2015) 15217–15224.
- [39] H.J. Li, J.Z. Du, X.J. Du, C.F. Xu, C.Y. Sun, H.X. Wang, Z.T. Cao, X.Z. Yang, Y. H. Zhu, S.M. Nie, J. Wang, Stimuli-responsive clustered nanoparticles for improved tumor penetration and therapeutic efficacy, *Proc. Natl. Acad. Sci. U.S.A.* 113 (2016) 4164–4169.
- [40] Z.J. Zhang, X. Zhang, X.H. Xu, Y.K. Li, Y.C. Li, D. Zhong, Y.Y. He, Z.W. Gu, Virus-inspired mimics based on dendritic lipopeptides for efficient tumor-specific infection and systemic drug delivery, *Adv. Funct. Mater.* 25 (2015) 5250–5260.
- [41] Z. Poon, D. Chang, X.Y. Zhao, P.T. Hammond, Layer-by-layer nanoparticles with a pH-sheddable layer for in vivo targeting of tumor hypoxia, *ACS Nano* 5 (2011) 4284–4292.
- [42] K.Y.Y. Fung, G.D. Fairn, W.L. Lee, Transcellular vesicular transport in epithelial and endothelial cells: challenges and opportunities, *Traffic* 19 (2018) 5–18.
- [43] S. Miura, H. Suzuki, Y.H. Bae, A multilayered cell culture model for transport study in solid tumors: evaluation of tissue penetration of polyethyleneimine based cationic micelles, *Nano Today* 9 (2014) 695–704.
- [44] H.L. Jang, S. Sengupta, Transcellular transfer of nanomedicine, *Nat. Nanotechnol.* 14 (2019) 731–732.
- [45] C.C. Zhang, E. Gau, W.J. Sun, J.Z. Zhu, B. Schmidt, A. Pich, X.Y. Shi, Influence of size, crosslinking degree and surface structure of poly(N-vinylcaprolactam)-based microgels on their penetration into multicellular tumor spheroids, *Biomater. Sci.* 7 (2019) 4738–4747.
- [46] X. Zhang, R.B. Bai, Surface electric properties of polypyrrole in aqueous solutions, *Langmuir* 19 (2003) 10703–10709.
- [47] D.J. Wu, L.X. Zhu, Y. Li, X.L. Zhang, S.M. Xu, G.S. Yang, T. Delair, Chitosan-based colloidal polyelectrolyte complexes for drug delivery: a review, *Carbohydr. Polym.* 238 (2020) 116126.
- [48] X. Li, M.S. Yang, X. Shi, X.X. Chu, L. Chen, Q. Wu, Y.Y. Wang, Effect of the intramolecular hydrogen bond on the spectral and optical properties in chitosan oligosaccharide, *Phys. E* 69 (2015) 237–242.
- [49] T.X. Miao, J.Q. Wang, Y. Zeng, G. Liu, X.Y. Chen, Polysaccharide-based controlled release systems for therapeutics delivery and tissue engineering: from bench to bedside, *Adv. Sci.* 5 (2018) 1700513.
- [50] V. Adibnia, M. Mirbagheri, P.L. Latreille, J. Faivre, B. Cecyre, J. Robert, J. F. Bouchard, V.A. Martinez, T. Delair, L. David, D.K. Hwang, X. Banquy, Chitosan hydrogel micro-bio-devices with complex capillary patterns via reactive-diffusive self-assembly, *Acta Biomater.* 99 (2019) 211–219.
- [51] Y. Zhuang, L.Z. Zhou, L.F. Zheng, Y. Hu, L. Ding, X. Li, C.C. Liu, J.H. Zhao, X.Y. Shi, R. Guo, LAPONITE-polyethylenimine based theranostic nanoplatform for tumor-targeting CT imaging and chemotherapy, *ACS Biomater. Sci. Eng.* 3 (2017) 431–442.
- [52] X. Li, L.X. Xing, Y. Hu, Z.J. Xiong, R.Z. Wang, X.Y. Xu, L.F. Du, M.W. Shen, X.Y. Shi, An RGD-modified hollow silica@Au core/shell nanoplatform for tumor combination therapy, *Acta Biomater.* 62 (2017) 273–283.
- [53] A.S. Chauhan, N.K. Jain, P.V. Diwan, Pre-clinical and behavioural toxicity profile of PAMAM dendrimers in mice, *Proc. R. Soc. London, Ser. A* 466 (2010) 1535–1550.
- [54] F. Danhier, To exploit the tumor microenvironment: since the EPR effect fails in the clinic, what is the future of nanomedicine? *J. Contr. Release* 244 (2016) 108–121.